Numerical and experimental investigation of an airfoil with load control in the wake of an active grid

A Fischer[1], T Lutz[1], E Krämer[1], U Cordes[2], K Hufnagel[2], C Tropea[2], G Kampers[3], M Hölling[3] and J Peinke[3]

[1]Institute of Aerodynamics and Gas Dynamics, University of Stuttgart, 70569 Stuttgart, Germany
[2]Institute of Fluid Mechanics and Aerodynamics, Technische Universität Darmstadt, 64287 Darmstadt, Germany
[3]ForWind and Institute of Physics, University of Oldenburg, 26111 Oldenburg, Germany

fischer@iag.uni-stuttgart.de

Abstract. A new passive load reduction system, using coupled leading and trailing edge flaps, was developed at TU Darmstadt and investigated experimentally and numerically. The experiments were performed in the wind tunnel of the University of Oldenburg, where sinusoidal inflow conditions, representing for example the tower blockage effect, were created by means of an active grid. The numerical investigations were performed at the University of Stuttgart, using a quasi two-dimensional setup and a block structured CFD solver. In the present paper, a brief description of the experimental setup is given, whereas the numerical setup, in particular the realisation of the wind tunnel conditions, is presented in more detail. Moreover, a comparison between the measured and simulated loads for an airfoil with and without adaptive camber concept is discussed.

1. Introduction

The operational environment of wind turbines is characterized by unsteady load fluctuations, caused by unsteady inflow conditions (e.g. atmospheric turbulence, wake turbine interaction, complex terrain, yawed inflow) and by the wind turbine itself (e.g. tower blockage) [1], [2], [3], [4], [5]. As these loads can cause higher fatigue and subsequently reduce life time of the turbines, they have to be alleviated to reduce the cost of energy and to increase the competitiveness of wind power against conventional sources of energy. Moreover, a further upscaling of the rotor to gain more energy per turbine is only possible, if loads can be reduced.

A promising concept to reduce load variations on wind turbine blades is the adaptive camber concept, developed by B. Lambie and K. Hufnagel at TU Darmstadt [6]. Leading and trailing edge flaps, which are coupled mechanically, adapt the camber of the airfoil passively to the inflow conditions until a moment equilibrium is achieved. Within the present study, an airfoil equipped with this concept was investigated in the wind tunnel of the University of Oldenburg. In order to test its behavior and ability to reduce load fluctuations caused by angle of attack (AoA) fluctuations due to a vertical gust, unsteady inflow was applied by an active grid.

The adaptive camber airfoil, including the wind tunnel environment, was also investigated numerically by means of two-dimensional CFD simulations. Comparisons between the experimental and numerical inflow conditions as well as load fluctuations, caused by AoA variations, and the ability of the load alleviation system to reduce these fluctuations are presented within this paper.

2. Approach and methods

2.1. Adaptive camber airfoil

The wind tunnel model of the airfoil used in the present investigation was manufactured at TU Darmstadt and has a chord length of $c = 0.18m$ and a span of $b = 0.8m$. It is a Clark-Y airfoil, equipped with mechanically coupled leading and trailing edge flaps (Figure 1). This airfoil was chosen because of the good leading and trailing edge flap effectiveness within the required range of deflections and its ability to provide attached flow for low Reynolds numbers. The second property was important for the design of a model wind turbine [7], which is also investigated in the frame of the DFG 780 project. In order to be consistent within the project, the Clark-Y was chosen for the present experimental setup, too. In the present investigation, the hinge locations of the leading and trailing edge flap are located at $x_{LE} = 0.2c$ and $x_{TE} = 0.7c$, respectively and a coupling ratio of $n = 3$ between the flaps was used. For this ratio, a counter clockwise deflection of $\gamma = 1°$ of the leading edge flap leads to a clockwise deflection of $\beta = 3°$ of the trailing edge flap. This combined movement is equivalent to a change in camber, whereby a positive deflection of leading and trailing edge flap leads to an increase of the camber and consequently to a higher lift. Figure 2 shows the c_p-distribution for a rigid airfoil at $\alpha = 0°$ and $\alpha = 5°$ as well as the distribution for an airfoil with deflected flaps. At higher AoA the forces on the trailing edge flap, but especially on the leading edge flap, are higher, leading to a de-cambering of the airfoil until an equilibrium between aerodynamic moment and the mechanical moment of the coupling mechanism is reached.

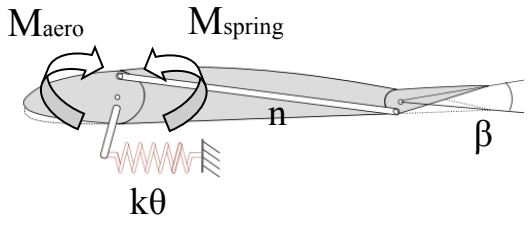

Figure 1. Adaptive camber mechanism.

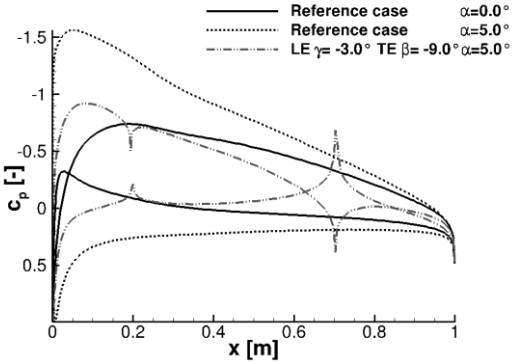

Figure 2. Inviscid c_p-distribution, calculated with XFOIL, for different AoA and flap deflection angles.

Figure 3 shows steady polars with and without deflected flaps. For a positive deflection of the trailing and leading edge flap the same lift coefficient can be achieved for a smaller angle of attack compared to the rigid airfoil. For a negative deflection it is vice versa. Consequently, with the adaptive camber concept, the gradient of the polar can be reduced over a wide range of AoA. In Figure 4 airfoil polars of the Clark-Y are displayed, showing a good effectivity of the flaps for positive and negative flap deflections. The Clark-Y´s ability to reduce load variations was already investigated experimentally under steady inflow conditions [6] and dynamic inflow conditions [8], [9] and numerically under steady inflow conditions [10] and showed good efficiency.

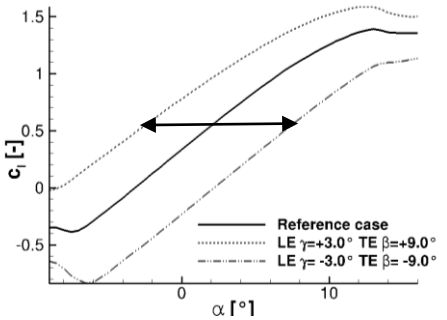

Figure 3. Steady c_l-α-polar, calculated with XFOIL ($Re = 0.187e6$), for different flap deflection angles.

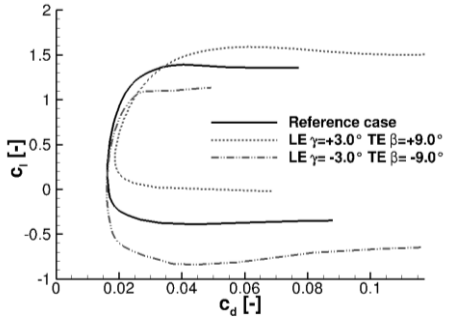

Figure 4. Steady c_l-c_d-polar, calculated with XFOIL ($Re = 0.187e6$), for different flap deflection angles.

2.2. Sinusoidal inflow conditions

Wind turbines experience a huge number of load fluctuations during their life time. The tower blockage effect for example has an important impact on the fatigue loads of wind turbines. Investigations of the NREL 5MW wind turbine, as used in the KIC-OFFWINDTECH project [11], [12] show, that the load fluctuations, caused by this effect, occur from approximately 160° - 210° azimuth, [5]. Thereby, the azimuth angle represents the position of the blade. At 0° the blade is in an upright position and at 180° it is located in front of the tower. Angle of attack extractions of the three-dimensional CFD simulation at rated condition under uniform inflow show that the tower blockage effect causes sinusoidal AoA variations of approximately $\pm 0.5°$. Angle of attack variations caused for example by gusts or yaw misalignment can lead to even higher AoA variations then seen in front of the tower.

The angle of attack fluctuations used in the experiment and in the numerical setup are periodical. With an excitation frequency of $f_{ex} = 6Hz$, an inflow velocity of $u = 16\,^{m}/_{s}$ and the chord length of $c = 0.18m$ of the airfoil the same reduced frequency as created by the tower blockage effect at 75% of the radius of the NREL wind turbine ($k \approx 0.212$) under uniform inflow (Case B1.2 in the KIC-OFFWINDTECH project [11]) was achieved for the present investigations. The amplitude of the fluctuations in the experiment was chosen significantly higher than the one caused by the tower blockage effect in order to receive significant effects. The Reynolds number in the experiment for this velocity amounts $Re(l_{chord}) = 0.187e6$ whereas the Reynolds number at 75% of the radius of the NREL wind turbine is approximately 100 times bigger. However, in the present investigations the aim was to match the reduced frequency and not the Reynolds number.

2.3. Experimental setup

The wind tunnel of the University of Oldenburg has an outlet nozzle of $0.8\,x\,1.0\,m^2$ ($h \times$ b) and a closed test section of $2.6m$ length. Unsteady inflow conditions are generated by means of an active grid, which is located upstream of the test section. The active grid consists of nine vertical and seven horizontal axes, with in total 126 mounted square flaps. Each axis can be controlled individually by stepper motors with a maximum rotational speed of $900°s^{-1}$. Thus, distinct inflow conditions can be generated and repeated with different actuation protocols for the grid. In the present study, the horizontal axes are fixed at 0° (flaps parallel to the flow) and only the vertical axes are actuated to generate flow angle fluctuations. Further information about the active grid can be found in [13] and [14].

The airfoil is mounted vertically, $1.055m$ downstream of the active grid (Figure 5) and was not tripped. Aerodynamic forces of interest are measured with two ME Systeme K3D120 3-component load cells, which are rigidly fixed to the airfoil axes. A Kuebler 5850 series 13-bit rotary encoder located at the bottom axis is used to measure the airfoil´s pitch angle.

Figure 5. Experimental setup [9].

2.4. Numerical setup

The quasi two-dimensional URANS simulations were performed using FLOWer, a block structured code developed by the German Aerospace Center (DLR) [15], which solves the compressible Navier-Stokes-Equations. The code version used for the present investigations has extensions, developed at the Institute of Aerodynamics and Gas Dynamics (IAG) of the University of Stuttgart, enabling amongst other flap deflections and overlapping meshes. Therefore it was possible to mesh the wind tunnel and the airfoil separately, using the overset grid technique according to [16].

To verify the numerical setup, a grid convergence study according to Celik [17] was performed. Three different setups were used in order to determine the grid convergence index (GCI_{fine}^{21}), which estimates the error caused by the numerical grid, as well as the extrapolated error e_{ext}^{2} between the value of the medium grid and the extrapolated value of a theoretically ideal mesh. Table 1 shows an extract from the GCI study.

Table 1. Extract from the grid convergence study for the force coefficient in y direction (c_y).

Cell number N_1, N_2, N_3	242,159; 138,980; 79,764
Extrapolated error of the medium grid e_{ext}^{2}	0.17%
Grid convergence index GCI_{fine}^{21}	0.21%

The values of the force coefficient are very low, indicating that the grid resolution of the medium grid is sufficient for the investigation of c_y. After the grid convergence study, the database of the airfoil mesh was improved to achieve a smoother c_p-distribution for future simulations.

The wind tunnel walls are realized as no slip walls and the inflow as a Dirichlet inflow condition [1]. The grid of the wind tunnel was extended in order to prevent a possible influence of the outflow boundary condition, which is realized as a farfield, on the test section (Figure 6).

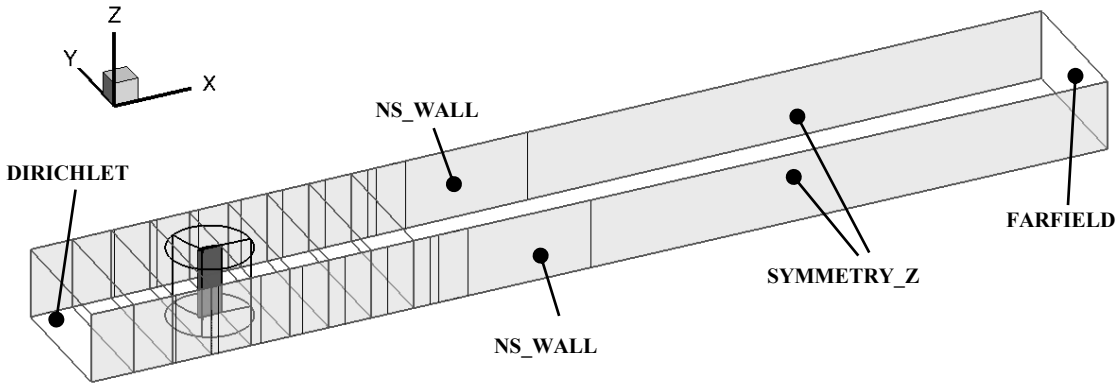

Figure 6. Boundary conditions and block borders of the numerical setup.

The airfoil was meshed with an O-grid, has no-slip walls and a fully resolved boundary layer, ensuring $y^+ < 1$ of the first layer. The whole setup has approximately 280,000 cells. A fully turbulent flow

about the airfoil and the Menter SST turbulence model were chosen for the simulations and a dual time stepping scheme [18] is used for the temporal discretization with 100 time steps per convective time unit and 25 inner iterations. At a frequency of $f = 6Hz$, a full period is resolved with approximately 1480 time steps. In the simulation, the flap deflection is prescribed with a Fourier series with seven Fourier coefficients, using deflection angles extracted from the measurements. The flap itself is realized as grid deformation which is based on radial basis functions [19], [20]. For the present investigations, 20,000 time steps, which correspond to approximately 13 periods, were simulated for the empty wind tunnel as well as for the rigid airfoil. For the flexible airfoil, a restart from the rigid case after 10,000 time steps was performed, simulating 20,000 further time steps.
The setup including wind tunnel and airfoil has been computed on 12 cpus and the simulation of 10,000 time steps with 25 inner iterations consumes approximately 260 cpuh.

3. Results

3.1. Reproduction of the sinusoidal inflow conditions in the numerical setup

In the experiment, the flow field in the empty wind tunnel was scanned with x-wires at 17 locations for an inflow velocity of approximately $8.5\,{}^{m}/_{S}$ ($Re(l_{chord}) = 0.100e6$), in order to characterize the flow field in the wind tunnel. The coordinate origin lies in the middle of the wind tunnel at the intended position of the airfoil leading edge. The x-axis points in the mean flow direction, z upwards along the blade span and y completes the right hand system. Seven points were measured in z-direction at the intended airfoil position at $\mathrm{y} = 0\mathrm{m}$ from $z = 0.05m$ to $0.35m$. Those measurements showed, that the two dimensionality of the flow field in z-direction is sufficient to justify the two dimensional numerical approach (Figure 7).

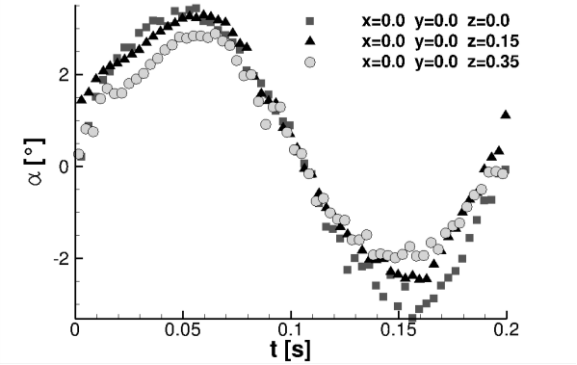

Figure 7. Angle of attack variations at the intended airfoil position at different z positions. The values were calculated from the phase averaged u and v components of the hot wire measurements.

Moreover, seven locations at the intended airfoil position at $z = 0m$ from $y = 0.05m$ to $0.35m$ and three positions on the centreline of the setup at the intended airfoil position ($x = 0m$), as well as at $x = 0.47m$ and $x = 0.74m$ upstream of the leading edge, were measured. These measurements were used to adapt the numerical inflow condition to achieve the same fluctuations as in the experimental setup. The investigations of the airfoil with and without the adaptive camber concept were performed at an inflow velocity of $u = 16\,{}^{m}/_{S}$. For this case, x-wire measurements in the empty wind tunnel were only performed in the middle of the test section at the intended airfoil position ($x = y = z = 0m$).
In the numerical setup, u and v fluctuations are propagated into the wind tunnel from the Dirichlet inflow boundary condition. 80 time steps per period are fed into the numerical domain. The fluctuations are generated with the following formulae:

$$u = \bar{u} + \Delta u \cdot \sin\left(2\pi f_{ex} \cdot \left(t + \frac{T_{period}}{2} \cdot\right)\right) \quad (1)$$

and

$$v = \bar{u} \cdot \sin(\Delta\alpha_{insert} \cdot \sin(2\pi f_{ex} \cdot t)). \quad (2)$$

The mean value of the velocity component in x-direction, $\bar{u}$, is the integral average of the time series and is $= 16.03\,{}^{m}/_{s}$ for the present setup. The fluctuation of the x component corresponds to the amplitude of the phase averaged signal and amounts $\Delta u = 0.66\,{}^{m}/_{s}$. In the present case, the excitation frequency is $f_{ex} = 6Hz$ and t is the current time. To ensure a phase shift of π between u and v at the inlet, $\frac{T_{period}}{2}$ was added to the current time.

The target value of the mean flow angle fluctuation was intended to be $\bar{\alpha} = 0°$. From the phase averaged signals of the two measured velocity components, the value of the flow angle amplitude at the intended airfoil position amounts $\Delta\alpha = 7.90°$ for the measurement and the simulation and was derived with the following formula:

$$\alpha = atan\left(\frac{v}{u}\right) \tag{3}$$

Because of the higher dependency of α from v and the conversion of the velocity components into each other inside of the wind tunnel, which will be explained in the following paragraphs, a higher flow angle fluctuation has to be applied at the inlet. The magnitude was iterated with several simulations and for the present setup amounts $\Delta\alpha_{insert} = 12.58°$. The connection between $\Delta\alpha_{insert}$ and the flow angle fluctuations at the intended airfoil position depends, among other things, on the flow velocity and the excitation frequency.

Because of the active grid, the mass flow within the wind tunnel is not constant, leading to u fluctuations in the whole tunnel, which are related to pressure fluctuations. Consequently, these variations are transported with speed of sound, leading to almost the same value of u at different x locations in the middle of the wind tunnel for a distinct time. However, v is transported with u in the wind tunnel, leading to a phase shift for v for different locations along the centreline of the wind tunnel. At the intended airfoil position, the u and v fluctuations are almost in phase for the present case, although they have a phase shift of π at the wind tunnel inlet. Figure 8 and 9 show representative simulated u and v fluctuations at the inlet and at the intended airfoil position. Representative measured fluctuations at the intended airfoil position are shown in Figure 10.

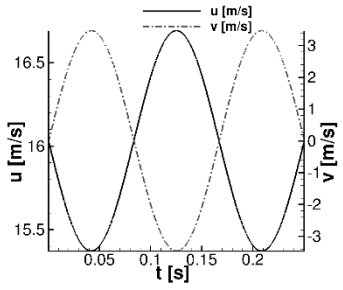

Figure 8. Simulated u and v variations at the wind tunnel inlet ($x = -1.055m$).

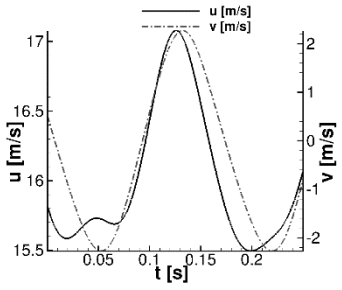

Figure 9. Simulated u and v variations at the intended airfoil position ($x = 0.0m$).

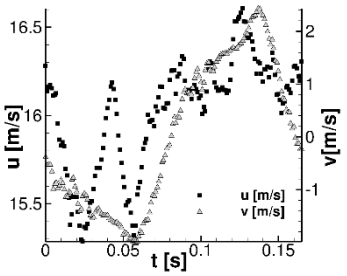

Figure 10. Measured phase averaged u and v variations at the intended airfoil position ($x = 0.0m$).

Going from the middle of the wind tunnel along the y-axis to the wind tunnel walls, the amplitudes of the simulated v fluctuations are getting smaller. Towards the lower side of the tunnel, the amount of the negative fluctuations decrease, as the wall prevents the flow from going downward. On the upper wall, it is vice versa (Figure 11). The same can be seen for the simulated flow angle leading to the conclusion, that it is more dependent on v than on u.

The u fluctuations are getting stronger for a higher wall proximity (Figure 12), leading to the conclusion, that the v fluctuations are transferred to u fluctuations. Moreover, in y-direction, the u component shows a time shift depending on the position.

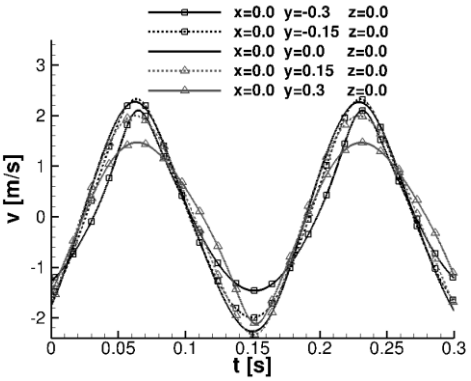

Figure 11. Representative, simulated v variations at different y positions.

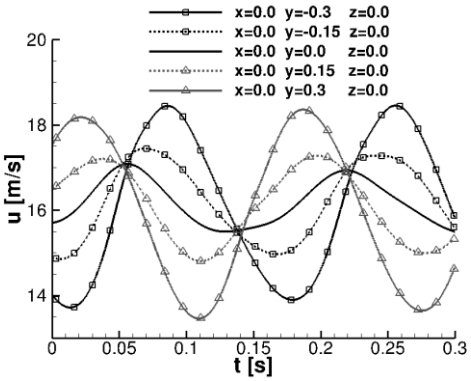

Figure 12. Representative, simulated u variations at different y positions.

A maximum of the flow angle leads to an expansion of the stream traces at the bottom of the wind tunnel ($y < 0$) (Figure 13 and Figure 14) and consequently to a reduction of u. On the upper wall, the stream traces are getting compressed, leading to a higher velocity component in x-direction. Therefore, the phase shift of u between $y > 0$ and $y < 0$ is almost π. Moreover, in Figure 13 it can be seen, that the v fluctuations, and consequently the α fluctuations, are strongest in the middle of the wind tunnel, whereas the u fluctuations are stronger near the walls (Figure 14).

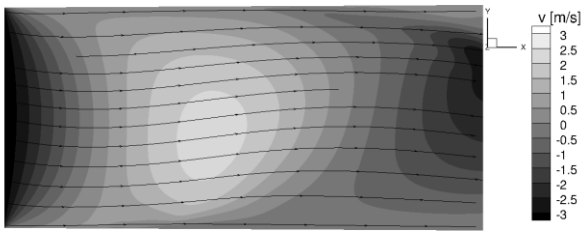

Figure 13. Simulated flow field with stream traces. Contour indicating the v component.

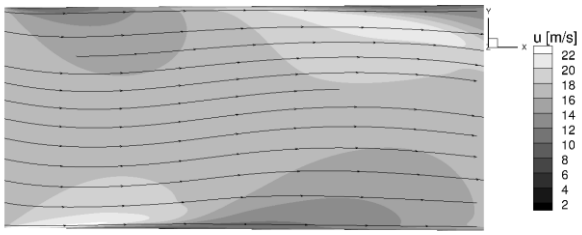

Figure 14. Simulated flow field with stream traces. Contour indicating the u component.

3.2. Investigation of the adaptive camber concept

For the present investigations, the flow angle variation shows a good accordance between the measurement and the simulation (Figure 15). A representative section of the simulated and measured flow angle fluctuations, along with a phase averaged signal of the measurement can be seen there. The sampling frequency of the hot wire measurement amounts $f_{sample} = 2kHz$ and the signal has a length of 30 $seconds$. For the case under investigation, the installation angle of the airfoil is $\alpha_{install} = 2.0°$. Over almost the whole range of flow angle variation ($\Delta\alpha \approx 8°$), the airfoil operates in the linear regime of the polar (Figure 16).

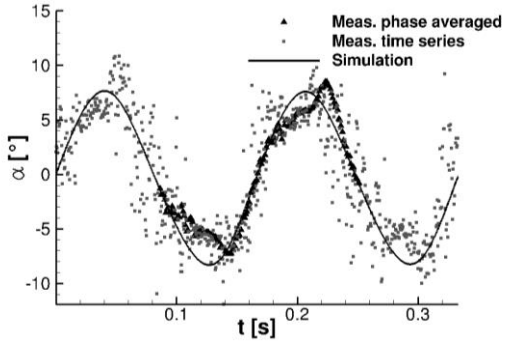

Figure 15. Flow angle variation, comparison between experiment and simulation at the intended airfoil position.

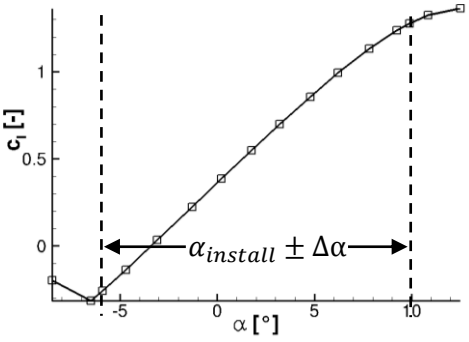

Figure 16. Steady polar (simulated) in the wind tunnel, including flow angle amplitude.

Lift and drag are defined as the forces perpendicular and parallel to the inflow velocity of an airfoil. In the present investigations, the inflow direction varies and consequently the orientation of lift and drag in the inertial system varies, too. Therefore, the force in the wind tunnel y-direction was evaluated instead of the lift. This force is representative for the load fluctuations caused by flow angle variations and is therefore a characteristic parameter for the evaluation of the load alleviation system.
Figure 17 shows the results of a FFT analysis for the measured force in y-direction per meter for the rigid airfoil and for the airfoil with adaptive camber (flexible airfoil). The transformation was done with a time series of the force with a sampling frequency of $f_{sample} = 1kHz$ over a signal of approximately 30 $seconds$, ensuring an integer number of periods within the signal. The signal was cut off at a frequency of $f_{cut-off} = 25Hz$.

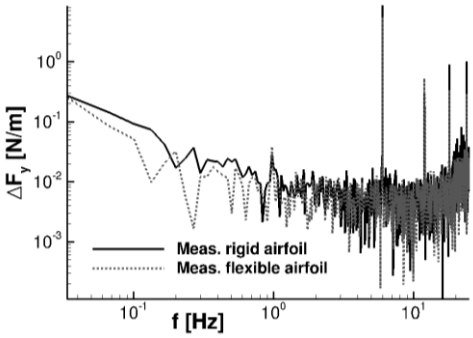

Figure 17. FFT of the measured F_y for the rigid and flexible case.

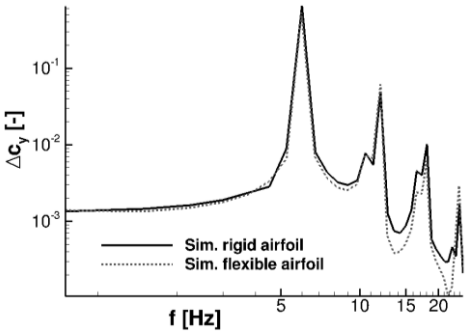

Figure 18. FFT of the simulated c_y for the rigid and flexible case.

The mean value of the flexible airfoil ($\overline{F_{y,flexible}} = 18.03\,{}^{N}/_{m}$) is higher than for the rigid airfoil ($\overline{F_{y,rigid}} = 14.21\,{}^{N}/_{m}$). This is because of the fact, that the flap angle is positive over the whole measurement, leading to a higher camber of the flexible airfoil, compared to the rigid one. With an adjustment of the preload and the spring stiffness of the airfoil, the deflection angle could be changed in future measurement campaigns, in order to receive another mean camber of the flexible airfoil under the present inflow conditions.
The highest amplitude can be seen for a frequency of $6Hz$, which was also expected, as the excitation frequency is $f_{ex} = 6Hz$, too. Moreover, higher harmonic frequencies can be seen. At $6Hz$, the amplitude of the rigid case is higher ($\Delta F_{y,rigid}(6Hz) = 8.58\,{}^{N}/_{m}$) than for the flexible case ($\Delta F_{y,flexible}(6Hz) = 5.55\,{}^{N}/_{m}$), leading to a load reduction for the flexible airfoil of 35.31%.
A FFT was also performed for the simulation (Figure 18) for the force coefficient in y direction. Thereby, eight periods were used for the transformation and the same effects can be seen for the simulation. Since for this case only a smaller number of periods was investigated, a fewer number of frequencies could be resolved. In this case, the load reduction amounts 19.39% ($\Delta c_{y,rigid}(6Hz) = 0.655$, $\Delta c_{y,flexible}(6Hz) = 0.528$).
A comparison between measurement and simulation for the rigid airfoil can be seen in Figure 19. Figure 20 shows the comparison for the flexible case along with the trailing edge flap angle, which was derived from the measurements and applied to the simulation as prescribed flap deflection. The phase averaged signal of the force in y direction, as well as a representative period of the simulated c_y (both represented as Φ) are normalized with the corresponding mean value ($\bar{\Phi}$) and the amplitude of the rigid case ($\Delta\Phi_{rigid}$), leading to the parameter $\Delta\Phi_{norm}$, representing the normalized load, in order to compare the two signals.

$$\Delta\Phi_{norm} = \frac{\Phi - \bar{\Phi}}{\Delta\Phi_{rigid}}$$

This normalization was done, as it is difficult to determine the unsteady inflow conditions in the wind tunnel and therefore a conversion of the values was not feasible.

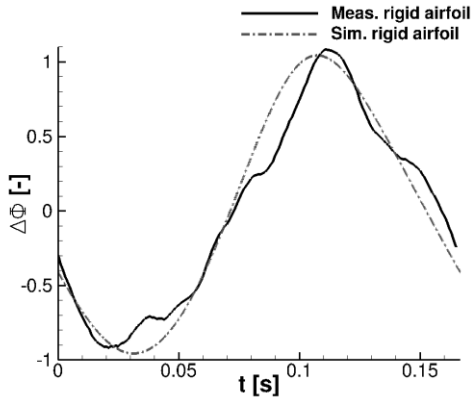

Figure 19. Comparison of the normalized loads between measurement and simulation for the rigid airfoil.

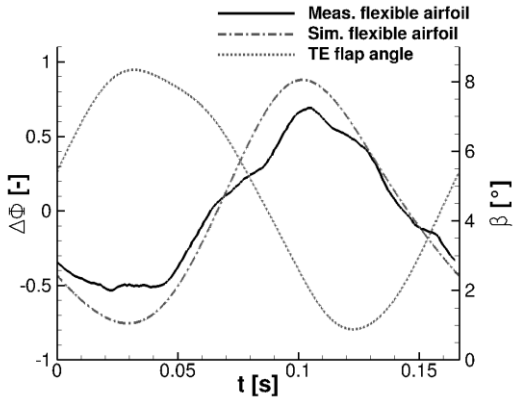

Figure 20. Comparison of the normalized loads between measurement and simulation for the flexible airfoil.

At $t \approx 0.11s$, where F_y respectively c_y reaches its maximum, the trailing edge flap angle β has its minimum. At this point, the camber of the flexible and of the rigid airfoil are almost similar for the present case, as β is close to zero. Consequently the values between the rigid and flexible case are closest. At $t \approx 0.03s$, β has its maximum and therefore the values are most different. A good accordance between the simulated and the measured signal can be achieved for the rigid case. However, the effectivity of the adaptive camber concept is better in the experiment, as the amplitude is smaller compared to the simulation.

As the rigid cases correspond very well and no separation occurs in the simulation, the only difference between the rigid and the flexible cases are the flap deflections. In the simulation, the force coefficient of the airfoil is calculated depending only on the aerodynamic forces whereas in the measurement not only the aerodynamics but also the inertia of the flaps is taken into account by the force measurements. This discrepancy between the load evaluation could lead to the present differences between the flexible cases.

4. Conclusions

An airfoil equipped with a new load alleviation concept, using coupled leading and trailing edge flaps for passive load reduction, and its behavior under sinusoidal inflow conditions, was investigated experimentally and numerically.

A grid convergence study was performed in order to estimate the error caused by the grid resolution and a detailed investigation of the velocities in the wind tunnel was done too. Thereby, the simulated velocity components in the wind tunnel were compared to hot wire measurements in order to ensure a good agreement between the flow conditions in simulation and experiment. A comparison of the hot wire measurements along the span of the airfoil showed, that the differences of the flow angle fluctuations are small enough to justify the quasi two-dimensional numerical approach. The comparison of the measured and simulated flow angle variations at the intended airfoil position showed an agreement of 99.32%.

Moreover, a comparison between the system response of the airfoil on the flow angle fluctuations between measurement and simulation showed a good accordance for the rigid case. However, the flexible case showed a higher load reduction in the measurement than in the simulation. Nevertheless, a significant reduction of the occurring load fluctuations, while maintaining a higher mean lift, was achieved in the experiment as well as in the simulation for the adaptive camber airfoil, showing a high potential of the concept for its use on wind turbine blades.

Acknowledgement
The present investigations were performed within the DFG PAK 780 project. The authors gratefully acknowledge the German Research Foundation (DFG) for funding the studies. The simulations have been carried out on the computational resource bwUniCluster funded by the Ministry of Science, Research and the Arts Baden-Württemberg and the Universities of the State of Baden-Württemberg, Germany, within the framework program bwHPC.

References

[1] Meister K, Lutz T and Krämer E 2014 *Journal of Physics: conference Series* vol 555
[2] Weihing P, Meister K, Schulz C, Lutz T and Krämer E 2014 *Journal of Physics: conference Series* vol 524
[3] Schulz C, Klein L, Weihing P, Lutz T and Krämer E 2014 *Journal of Physics: conference Series* vol 524
[4] Weihing P, Schulz C, Lutz T and Krämer E *High Performance Computing in Science and Engineering 14* (Springer)
[5] Schulz C, Fischer A, Weihing P, Lutz T and Krämer E *High Performance Computing in Science and Engineering 15* (Springer)
[6] Lambie B 2011 Aeroelastic investigation of a wind turbine airfoil with self-adaptive camber Doctoral thesis (Darmstadt)
[7] Pechlivanoglou G, Fischer J, Eisele O, et al. 2015 DEWEK (Bremen)
[8] Cordes U, Hufnagel K, Tropea C, Kampers G, Hölling M and Peinke J 2015 *AIAA Applied Aerodynamics Conference* (Dallas)
[9] Kampers G, Peinke J, Hölling M, Cordes U and Tropea C 2015 *AIAA Applied Aerodynamics Conference* (Dallas)
[10] Fischer A, Jost E, Lutz T and Krämer E 2014 *10th EAWE PhD seminar on Wind Energy in Europe* (Orléans)
[11] Bekiropoulos D, Lutz T, Baltazar J, Lehmkuhl O and Glodic N *2013 D2013-3.1: Comparison of benchmark results from cfd-simulation Deliverable report, KIC-OFFWINDTECH*
[12] Bekiropoulos D, Rieß R, Lutz T, Krämer E, Matha D, Werner M and Cheng P-W 2012 *DEWEK* (Bremen)
[13] Knebel P, Kittel A, Peinke J 2011 *Experiments in Fluids* 51, 471–481
[14] Weitemeyer S, Reinke N, Peinke J, Hölling M 2013 *Fluid Dynamics Research* 45(6), 061,407
[15] Kroll N and Fassbender J 2002 *MEGAFLOW Numerical Flow Simulation for Aircraft Design* (Berlin: Springer)
[16] Benek J, Steger J, Dougherty F and Buning P 1986 *Chimera. A Grid-Embedding Technique.*
[17] Celik I B, Ghia U, Roache P J, et al. 2008 *Journal of fluids {Engineering-Transactions} of the {ASME}*, 130(7)
[18] Jameson A 1991 *AIAA paper,* 1596
[19] Jost E, Fischer A, Lutz T and Krämer E 2014 *10th EAWE PhD seminar on Wind Energy in Europe* (Orléans)
[20] Schuff M, Kranzinger P, Keßler M and Krämer E 2014 *ERF2014 proceedings* (Rovereto)